Transient Temperature and Heat Flux Measurement in Ultrasonic Joining of Battery Tabs Using Thin-Film Microsensors

Hang Li

Hongseok Choi

Chao Ma

Jingzhou Zhao

Hongrui Jiang

Department of Mechanical Engineering,
University of Wisconsin-Madison,
1513 University Avenue,
Madison, WI 53706

Wayne Cai

Jeffrey A. Abell

Manufacturing Systems Research Lab,
GM Global R&D,
30500 Mound Road,
Warren, MI 48090-9055

Xiaochun Li

Department of Mechanical Engineering,
University of Wisconsin-Madison,
1513 University Avenue,
Madison, WI 53706
e-mail: xcli@engr.wisc.edu

Process physics understanding, real time monitoring, and control of various manufacturing processes, such as battery manufacturing, are crucial for product quality assurance. While ultrasonic welding has been used for joining batteries in electric vehicles (EVs), the welding physics, and process attributes, such as the heat generation and heat flow during the joining process, is still not well understood leading to time-consuming trial-and-error based process optimization. This study is to investigate thermal phenomena (i.e., transient temperature and heat flux) by using micro thin-film thermocouples (TFTC) and thin-film thermopile (TFTP) arrays (referred to as microsensors in this paper) at the very vicinity of the ultrasonic welding spot during joining of three-layered battery tabs and Cu buss bars (i.e., battery interconnect) as in General Motors's (GM) Chevy Volt. Microsensors were first fabricated on the buss bars. A series of experiments were then conducted to investigate the dynamic heat generation during the welding process. Experimental results showed that TFTCs enabled the sensing of transient temperatures with much higher spatial and temporal resolutions than conventional thermocouples. It was further found that the TFTPs were more sensitive to the transient heat generation process during welding than TFTCs. More significantly, the heat flux change rate was found to be able to provide better insight for the process. It provided evidence indicating that the ultrasonic welding process involves three distinct stages, i.e., friction heating, plastic work, and diffusion bonding stages. The heat flux change rate thus has significant potential to identify the in-situ welding quality, in the context of welding process monitoring, and control of ultrasonic welding process. The weld samples were examined using scanning electron microscopy (SEM) and energy dispersive X-ray spectroscopy (EDS) to study the material interactions at the bonding interface as a function of weld time and have successfully validated the proposed three-stage welding theory. [DOI: 10.1115/1.4024816]

Keywords: ultrasonic joining, battery manufacturing, thin-film thermal sensors, process monitoring

1 Introduction

1.1 Background. Battery electric vehicles are gaining momentum for automobile industry recently. For their successful commercialization, it is crucial to ensure high quality fabrication and assembly for the battery packs. A battery pack for EVs typically consists of a large number of battery cells that must be assembled together with robust joints to ensure mechanical and electrical properties. Efforts have been taken to investigate several joining technologies, such as resistance welding, laser welding, ultrasonic welding, and mechanical fastening [1,2]. Among all these techniques, ultrasonic welding, a solid state joining process, is widely regarded as one of the best for battery joining due to its capability of joining dissimilar, multiple, and thin layers at low temperatures [3–9].

Although ultrasonic metal welding (USMW) was invented in 1940s, its bonding mechanism is still not fully understood [10–13]. There are a few different theories proposed so far. Kodama proposed that the ultrasonic bonding process involves two steps [14]. In the first step, friction, as a result of the ultrasonic oscillation, causes mechanical cleaning and smoothing of the interface and initiates point bonding. In the second step, the relative motion between the workpieces induces a sudden plastic flow. In this theory, it is believed that the oxidation at the interface must be removed before bonding can be initiated. Several interrelated phenomena occur during USMW, including plastic friction heating, recrystallization, and interdiffusion, deformation and fatigue. However, it was suggested that USMW is a heat dependent process by some other investigators [15,16]. Plastic deformation takes place only when: (1) the relative displacement between the workpieces is sufficient to induce localized slip; (2) the resulting frictional stress is greater than the flow stress of the sublayer. Hazlett and Ambekar observed that bonds can be formed by mechanical mixing at the interface [17]. Moreover, diffusion observed is attributed to grain boundary diffusion as the temperature is not sufficiently high to result in bulk diffusion.

Recently, thermomechanical phenomena were studied by the use of embedded thin-film sensors for various manufacturing processes [18–24]. Two types of thin-film microsensors, K-type TFTC, and K-type thermocouple based TFTP, were designed and fabricated for in-situ temperature measurement of ultrasonic welding process to better understand the process [18,22]. The experiments were only conducted for ultrasonic joining two layers of materials, i.e., Cu and Ni [18]. Thus, it would be of interest to

Contributed by the Manufacturing Engineering Division of ASME for publication in the Journal of Manufacturing Science and Engineering. Manuscript received July 5, 2012; final manuscript received April 19, 2013; published online September 16, 2013. Assoc. Editor: Robert Gao.

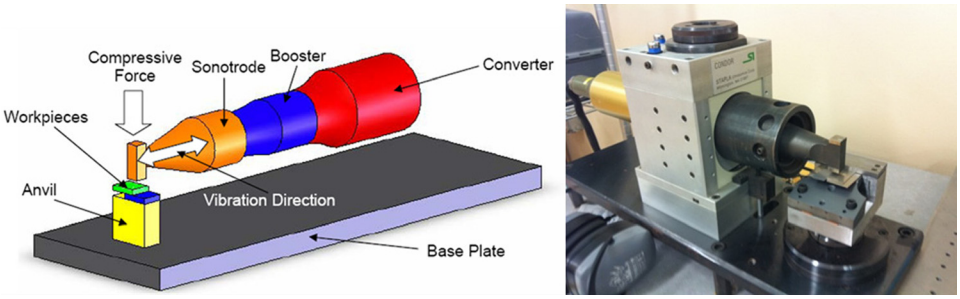

Fig. 1 Schematic of USMW machine and weld area and the actual machine

Fig. 2 USMW workpieces

study the ultrasonic joining of multilayer thin battery buss bars and tabs for battery assembly with thin-film microsensors.

In this paper, ultrasonic joining will be used to weld a three-layered thin sheet materials (Ni-coated Cu battery tab, 0.2 mm thick each layer) with a thicker bottom layer (Ni-coated Cu buss bar, 0.9 mm thick). Thin-film microsensors (TFTCs and TFTPs) will be fabricated directly on top of the thick Cu buss bar to study the heat generation and bonding mechanism for ultrasonic joining in battery assembly.

1.2 Ultrasonic Welder and Workpieces. A schematic of a STAPLA ultrasonic metal welder used in this study is shown in Fig. 1. There are three main welding parameters, namely, sonotrode vibration amplitude, clamping force, and welding time. The nominal operating frequency of the welder is 20 kHz with a maximum output electric power of 3 kW. The clamping force has a range from 311 N to 3536 N. Two different booster units are available to allow a zero-to-peak amplitude output from 10 to 40 μm. The maximum weld duration is 9 s, and the resolution is about 0.01 s.

Figure 2 shows the workpieces (Ni-coated Cu buss bars and tabs) and ultrasonic welded samples being used in GM Chevy Volt battery packs assembly. Three layers of Ni-coated Cu buss tabs (45 mm $\times$ 41 mm in size and 0.2 mm thick each layer) are to be welded to the Ni-coated buss bar (49 mm $\times$ 35 mm in size) of 0.9 mm thick to serve as an interconnect. A thin nickel coating ($\sim$2 μm) offers good corrosion resistance against acids, alkalis, and oxidizing agents.

2 Design, Fabrication, and Calibration of Thin-Film Microsensors

2.1 Design of Thin-Film Microsensor. Two different layouts of thin-film microsensor arrays were designed in this study, as illustrated in Fig. 3. Figure 3(*a*) shows that two TFTCs are located on a lower side of the welding spot. Two TFTCs ($TFTC_1$ and $TFTC_2$) and one TFTP are placed on the left side of the welding spot. The two TFTCs located in left of the weld spot can be used to calculate heat flux, which can be compared with the measured heat flux with the TFTP array. Moreover, two more TFTCs ($TFTC_3$ and $TFTC_4$) are placed in the middle but outside the welding zone. Figure 3(*b*) shows four TFTPs designed to investigate the proximity sensitivity of heat flux sensors. Four TFTCs are designed to validate the heat generation during ultrasonic joining process. All these four TFTCs and four TFTPs are placed on the left of the welding zone in the welding vibration direction. In both layout designs, the closest distance between the microsensors and the edge of the weld zone is 1.5 mm. Neighboring sensors are placed 1.5 mm apart. TFTCs have a sensor junction area (the overlapped area of two sensor legs) of 30 μm by 30 μm. The TFTP consists of 11 pairs of *K*-type TFTCs on each side to measure the average surface heat flux along the sonotrode vibration direction.

2.2 Sensor Fabrication on Cu Buss Bars. For the microfabrication of thin-film microsensors, the substrates should have a good surface finish, preferably with a surface roughness less than 100 nm. Surface topography of the Cu buss bar was evaluated using a white light interferometer. The buss bars typically had a rough surface finish with an Ra of about 0.2–0.35 μm and a peak-to-valley (PV) value of 2.7–3.3 μm, as shown in Fig. 4. To mitigate this problem, a layer of polyimide (PI) with a film thickness of 1 μm was coated on the Cu buss bar with a photoresist spinning machine (spinning for 10 s at 500 rpm and then spinning for 25 s at 2500 rpm). The PI film was then cured in a nitrogen-filled oven: heating with a ramp rate of 4 °C/min from room temperature to 200 °C, then holding for 30 min at 200 °C, again heating up to 300 °C with a ramp rate of 2.5 °C/min, holding at this temperature for 60 min, and finally cooling gradually to room temperature. With the PI film coating on the Cu buss bars, their surface was much smoother with typical surface values of 0.08 μm Ra and 0.8 μm PV, as shown in Fig. 5. It should be noted that the thin polyimide film can also serve as an insulation layer on the Ni-coated Cu buss bar to prevent thin-film microsensors from short circuit to the conductive substrates.

Thin-film microsensors fabrication procedure can be divided into six steps, as shown in Fig. 6. Figure 6(*1*) shows the exposure step. After the exposure, the photoresist S1813 was developed in the MF-321 developer. In Step 2, LOR-3 A, a nonphotosensitive material that dissolves in photo resist developer, was used to generate an undercut beneath S1813 as shown in Fig. 6(*2*). Then, a

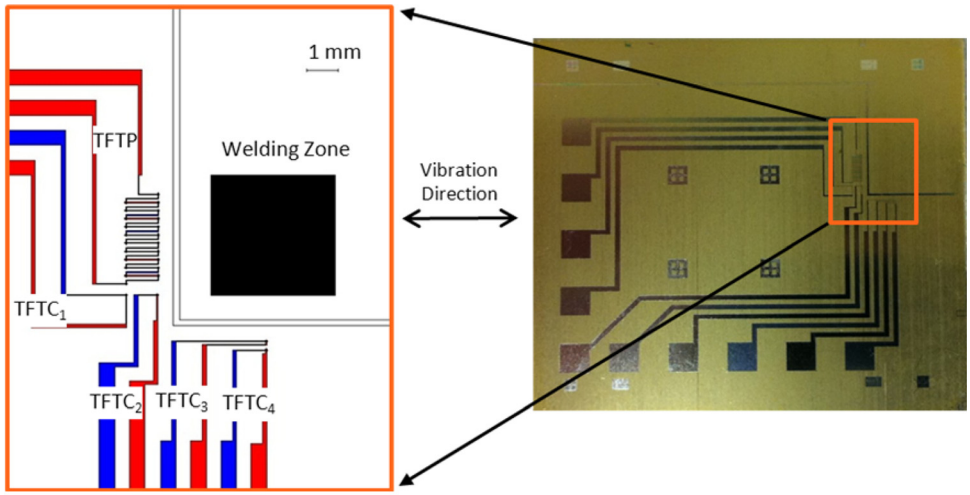

(a)

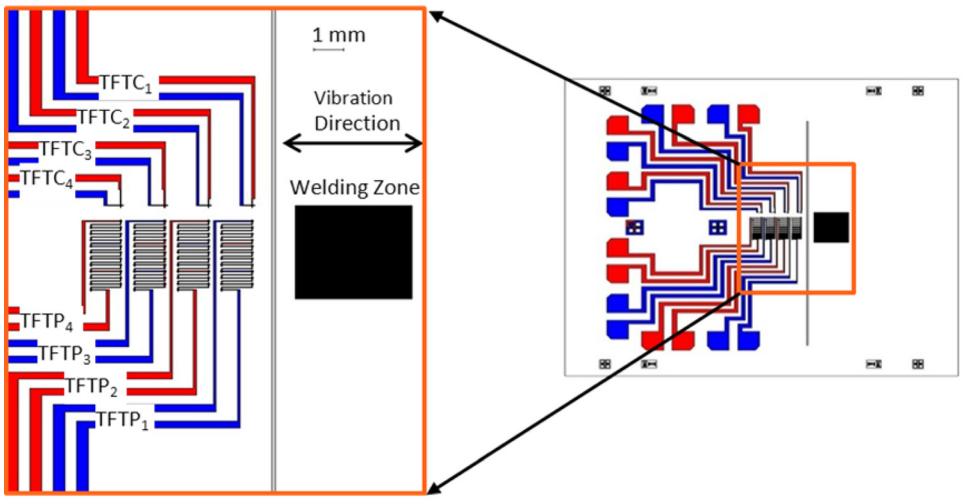

(b)

Fig. 3 Two different thin-film microsensor design layouts

thin film of chromel was deposited with a CVC 601 dc sputtering system, as shown in Fig. 6(*3*). In step 4, a subsequent lift-off process removed S1813 and LOR-3 A in acetone, as well as the extra chromel film deposited on S1813, resulting in a structure illustrated in Fig. 6(*4*). The steps were repeated in order to deposit an alumel leg, as shown in Figs. 6(*5*) and 6(*6*), respectively.

2.3 Sensor Calibration

2.3.1 Calibration for TFTCs. To examine the functionality and sensitivity of the fabricated *K*-type TFTCs, the sensors were calibrated from room temperature to about 700 °C in a temperature-controlled tube furnace. During the calibration process, an argon flow was maintained in the tube furnace. Two commercial *K*-type thermocouples were attached to the top and bottom of the substrate near the TFTC junction area, respectively, to serve as references. A National Instruments (NI) 6070 E data acquisition system (DAQ) from NI was used to collect data. The furnace was heated up gradually and allowed to stabilize at a number of preset temperatures. The substrate temperature was determined when the temperature difference between two

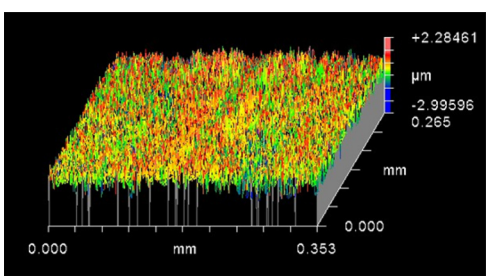

Fig. 4 Surface finish of as-received Cu buss bar

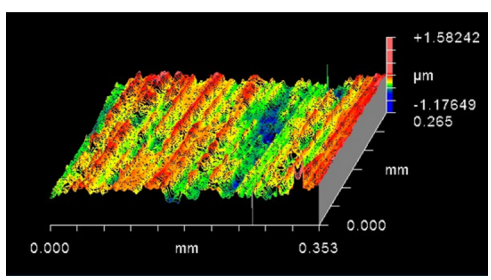

Fig. 5 Surface finish of Cu buss bar after PI coating

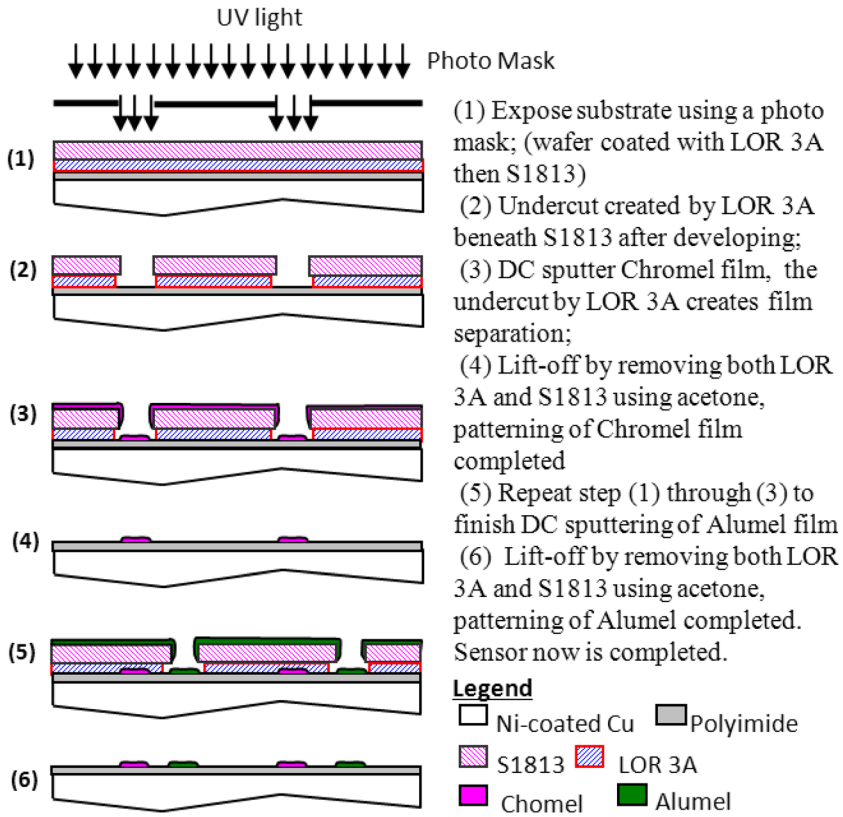

Fig. 6 Thin-film sensor fabrication process

reference thermocouples was smaller than 0.1 °C. Calibration results show that TFTC has a linear response and its thermoelectric sensitivity is determined as 41.4 μV/°C, which matches the theoretical value of a standard K-type thermocouple.

2.3.2 Calibration for TFTPs. The sensitivity of a thermopile, E_{sen}, usually expressed in a voltage output, V_{sen}, per heat flux (W/m^2), is related to the substrate material, the number of pairs of thermocouples as well as the distance between two junctions (e.g., ΔX shown in Fig. 7). The heat flux can be calculated by

$$Q = V_{sen}/E_{sen} \tag{1}$$

To characterize E_{sen} of the thin-film thermopile, a sensor unit was fabricated, as shown in Fig. 7. The thermopile unit has 11 pairs of K-type thermocouples on each side with a ΔX of 1 mm. Two standard wire thermocouples were attached to the substrate with a large separation distance (ΔL) of 16.5 mm to serve as the reference. The reference heat flux Q can then be calculated by using the following formula:

$$Q = K(\Delta T/\Delta L) \tag{2}$$

where ΔT is the temperature difference between the two reference thermocouples and K is the thermal conductivity of the copper

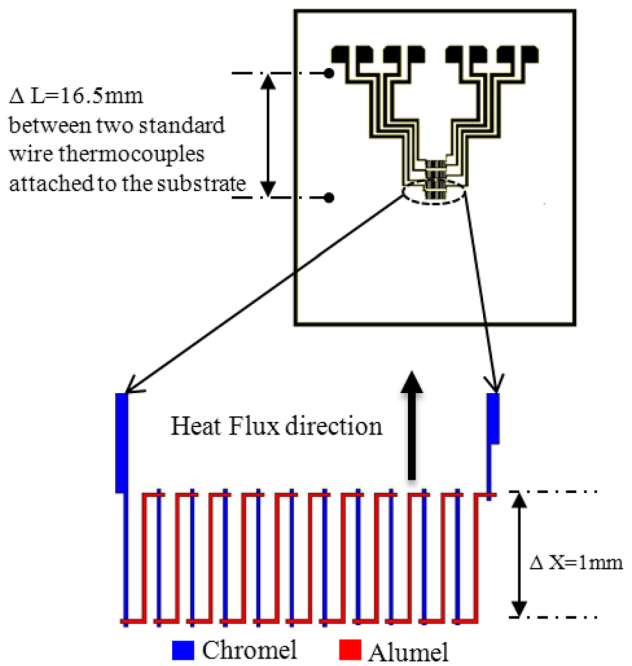

Fig. 7 TFTP unit for calibration (each sensor junction area: 30 μm by 30 μm)

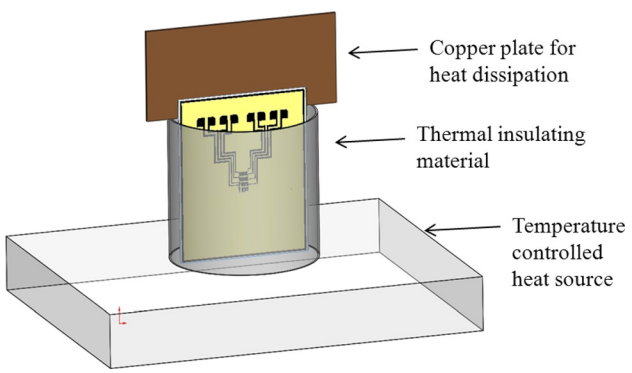

Fig. 8 TFTP calibration set up

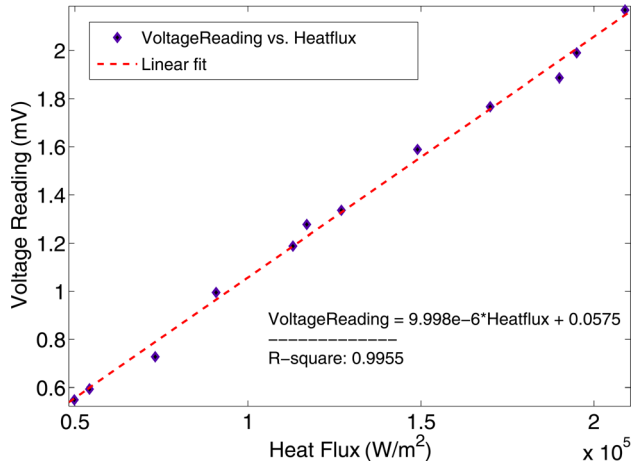

Fig. 9 Characterization of TFTP

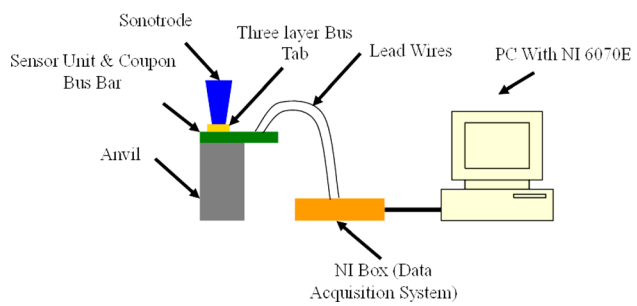

Fig. 10 Experimental setup for in-situ temperature and/or heat flux measurement

buss bar. Figure 8 shows the calibration setup. A temperature-controlled hot plate was used as the heat source on the hot side. The sensor unit was wrapped with a heat insulation material so that heat flow would be approximately guided in one direction. A large copper plate was attached to the other end of the sensor substrate using a thermal conductive adhesive (LOCTITE 383), serving as a heat sink to dissipate heat to generate a "cold" end. By controlling the hot plate at different temperatures, different heat flux was obtained. As shown in Fig. 9, the voltages from the TFTP are plotted against the reference heat flux Q to determine its sensitivity, E_{sen} to be 9.998×10^{-6} mV/(W/m^2), whereas the theoretical value was found to be 11.4×10^{-6} mV/(W/m^2).

3 Welding Experiments and Results

Ultrasonic welding experiment was conducted using a STAPLA ultrasonic metal welder as previously mentioned in Sec. 1. Three layers of Ni-coated Cu tabs (0.2 mm thick each layer) were welded to the 0.9 mm thick Ni-coated buss bar. Design of experiments was performed. Welding quality was determined by tension-shear tests. Optimized welding parameters were determined as welding duration at 1.2 s, vibration amplitude at 26 μm, and clamping pressure at 26 MPa. The temperature and/or heat flux data during welding were collected using a NI 6070 E DAQ system with a sampling rate of 10 kHz. Figure 10 shows the schematic setup for data acquisition. The lead wires that connect the microsensors to the data acquisition system are also K type thermocouple wires to make sure that the cold junction is at room temperature.

3.1 Temperature Measurement Results. Figure 11 shows representative measurement results (after noise filtering) from both the thin-film thermocouple and the thin-film thermopile

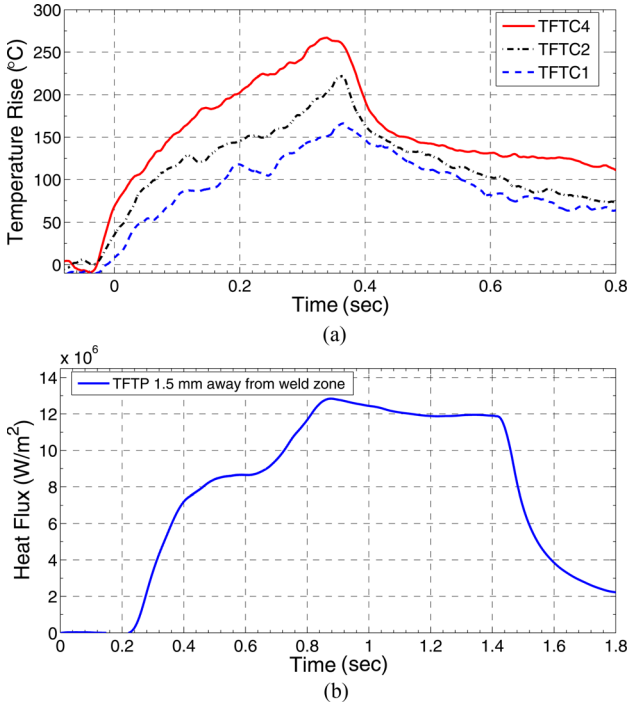

Fig. 11 In-situ temperature and heat flux measurement results during USMW

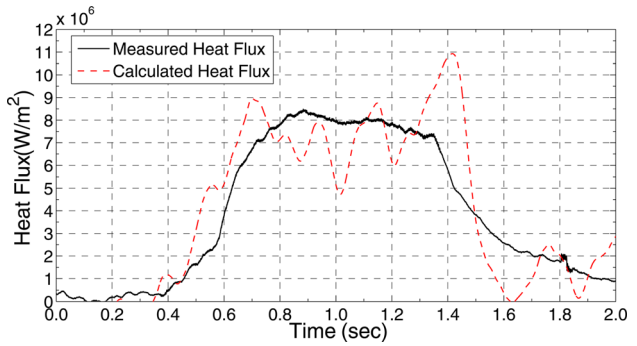

Fig. 12 Comparison between measured heat flux from TFTPs and the calculated one from two TFTCs

arrays. The locations of $TFTC_1$, $TFTC_2$, and $TFTC_4$ are shown in Fig. 3(*a*). Temperature rise measured by all TFTCs, as shown in Fig. 11(*a*), showed a similar pattern which indicates a drastic temperature rise at the initial stage and then the temperature rise slows down to reach a peak value. Figure 11(*b*) shows the heat flux measured by thin-film thermopiles.

3.2 Heat Flux Measurement Results. The design shown in Fig. 3(*a*) was used to compare the heat flux data acquired by TFTP with the heat flux calculated from the temperature difference between $TFTC_1$ and $TFTC_2$. The calculated heat flux matched the measured heat flux by TFTP in general, as shown in Fig. 12. However, the calculated heat flux is much noisier because a single TC is too noisy, making it unreliable for process control. Thus, only the heat flux signals from TFTPs will be used for process understanding.

The typical heat flux signals, as shown in Figs. 11(*b*) and 13(*a*), have some distinct features. By introducing heat flux change rate, which is the first derivative of heat flux over time, it reveals three distinct regions over time for the welding process, as shown in Fig. 13(*b*). This significant discovery suggests a three-stage

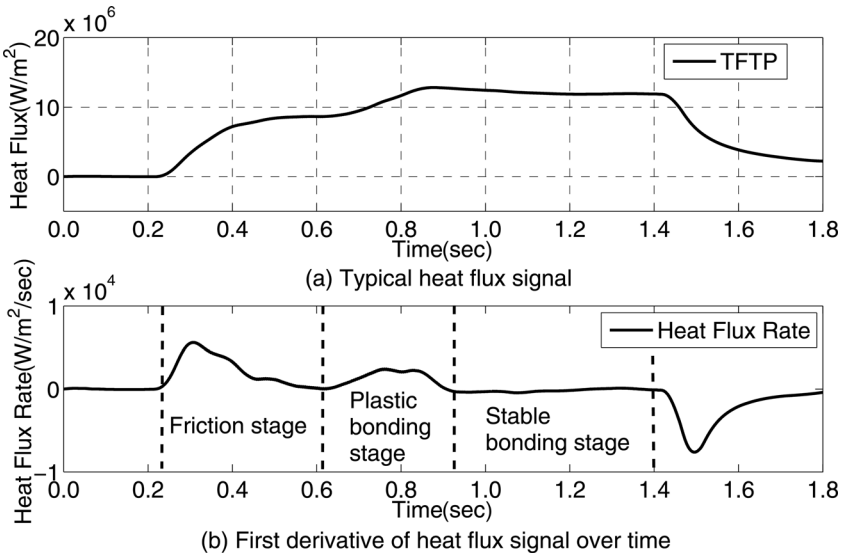

Fig. 13 Heat flux and heat flux change rate

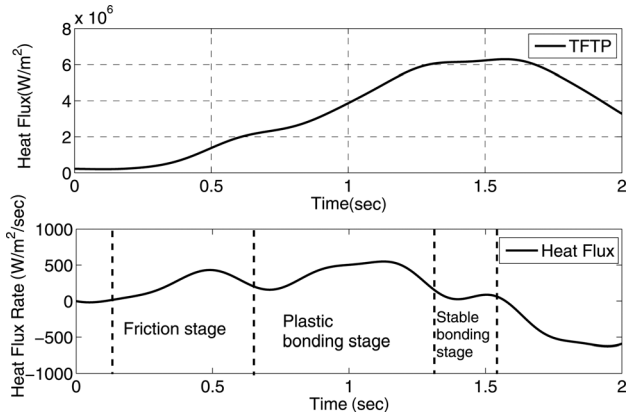

Fig. 14 Heat flux change rates for different TFTPs with 4.5 mm to welding zone

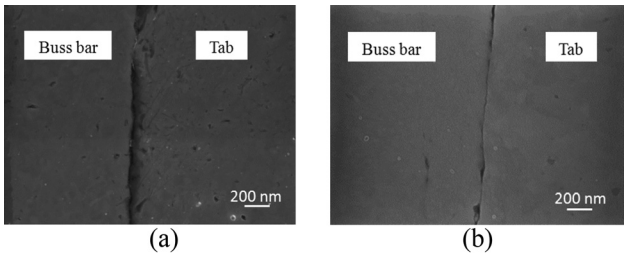

Fig. 15 SEM pictures of welding interfaces

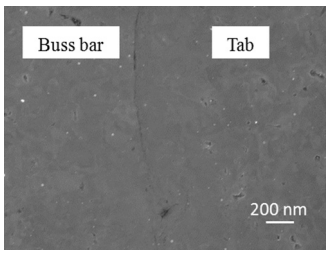

Fig. 16 SEM pictures of sample welded with a duration of 0.8 s

welding mechanism: friction heating, plastic work, and diffusion bonding stages.

From the application point view, further the micro heat flux sensors are placed away from the welding zone, easier the practical implementation can be carried out. Thus, a proximity sensitivity of the microsensors during welding was conducted. A typical result is shown in Fig. 14. A further study on the heat flux change rates indicates that TFTPs can still effectively capture the three stages even when it is located 4.5 mm away from the welding edge.

4 Validation of the Three-Stage Bonding Theory

To further investigate and validate the theory of three-stage bonding in ultrasonic welding as signaled by the heat flux change rate, weld microstructures were examined by SEM and EDS. Samples were prepared with various welding durations of 0.6 s, 0.8 s, 1 s, 1.2 s, and 1.5 s while maintaining other parameters at the optimized values. An unwelded sample was also used as reference.

The first peak of the heat flux change rate in Fig. 13(*b*) indicated that a large amount of heat was generated at the beginning of the process. This was due to the severe fretting and friction at the interface of two workpieces when the two surfaces are brought into close contact by a large pressure and forced into relative motion of high frequency (~20 kHz). The surface asperities and oxide were removed and dispersed at this stage, which resulted in a smoothened contact interface as shown in Fig. 15. Comparison between the interfaces of an unwelded sample (Fig. 15(*a*)) and a welded sample with a duration of 0.6 s (Fig. 15(*b*)) clearly showed the effect of this asperities removal and smoothing process. However, no trace of bonding is found at this stage. Note that Figs. 15–17 display only the Ni–Ni interfaces, since the bonding of two metals (i.e., 0.2 mm Ni-coated tab and 0.9 mm Ni-coated coupon) occurred between the two Ni coatings only (instead of Cu).

The friction stage ceases at around 0.6 s as shown in Fig. 13(*b*) at which point plastic working stage begins. Partial bonding/seizing develops at this stage as shown in the SEM picture of the welded sample with duration of 0.8 s (Fig. 16). Heat source in this stage is from the plastic deformation at the spots where bonding starts to form.

Plastically deformed interface resulted in even more intimate contact between mating surfaces where the interdiffusion takes

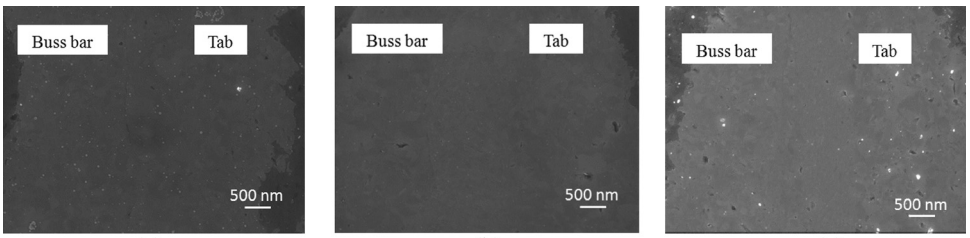

Fig. 17 SEM pictures of sample welded with duration (*a*) 1 s (*b*) 1.2 s, and (*c*) 1.5 s

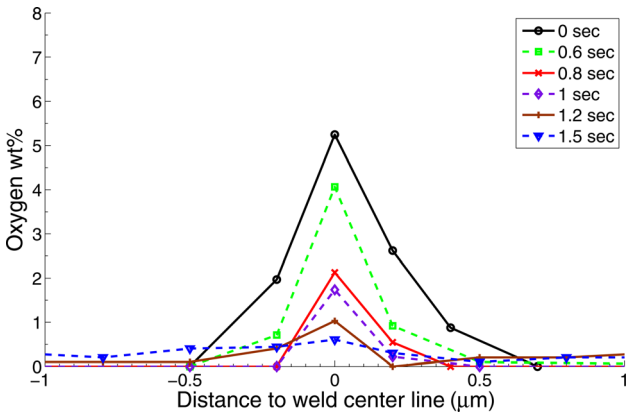

Fig. 18 Oxygen wt. % determined by EDS spot analysis across the welding center line

place more rapidly. The stable stage in the heat generation curve starts when the transient partial seizing grows to an almost seamless interface as shown in Fig. 17. Atomic diffusion then dominates this stage. It is evident that the bonding interface has grown from partial bonding to a full bond throughout the interface and no further change in microstructure can readily be observed in the SEM pictures.

Since it is very difficult to trace the Ni movement during the bonding process at the Ni–Ni interface, we examined the distribution of surface oxygen element (such as in the forms of Ni oxide) using spot EDS to infer the interfacial Ni mixing/diffusion, as shown in Fig. 18. It should be noted that gaps still exist between the tabs and the buss bar in the not-fully bonded samples (i.e., welding durations of 0 s and 0.6 s), leading to higher concentration of oxygen elements at the interface. It is evident that the diffusion of the oxygen element continues throughout the welding process in a fashion that the oxygen transports further away from the interface and becomes more uniformly distributed normal to the bonding interface line.

5 Conclusions

Thin-film microsensors (TFTCs and TFTPs) were successfully fabricated and utilized to measure transient temperature and heat flux during ultrasonic joining of Cu battery tabs and buss bars. The maximum temperature as measured by the thin-film microsensors on the Cu buss bar is 270 °C at a location about 1 mm away from the edge of the weld spot. The maximum heat flux is 1.3×10^7 W/m^2 as measured about 2.0 mm away from the weld spot. The heat flux change rate provides excellent insight to the ultrasonic welding mechanisms. Three distinct welding stages, namely, friction heating, plastic work, and diffusion bonding, were found existed during the ultrasonic welding process. Spot EDS was used to study the interfacial bonding evolution in ultrasonic welding process by examining the mixing/diffusion of surface oxide. The method validated our proposed three-stage bonding theory in ultrasonic welding. This study suggests that thin-film microsensors are capable of providing insights to the understanding of the welding physics. The thin-film microsensors could also have great potential for a robust process control of ultrasonic joining in battery manufacturing.

Acknowledgment

This work was supported by General Motors and Department of Energy.

References

[1] Lee, S. S., Kim, T. H., Hu, S. J., Cai, W. W., and Abell, J. A., 2010, "Joining Technologies for Automotive Lithium-Ion Battery Manufacturing: A Review," ASME Conf. Proc., Erie, PA, **1**, pp. 541–549.
[2] Kim, J., Yoo, S., and Kim, J., 2008, "Optimization of Welding Conditions for Sealing of Lithium-Ion Battery by Pulsed Nd:YAG Laser," Mater. Sci. Forum, **580–582**, pp. 523–526.
[3] Balandin, G. F., Kuznetsov, V. A., and Silin, L. L., 1967, "Fretting Action Between Members in Ultrasonic Welding of Metals," Weld. Prod., **10**, pp. 77–80.
[4] Gao, Y., and Doumanidis, C., 2002, "Mechanical Analysis of Ultrasonic Bonding for Rapid Prototyping," ASME J. Manuf. Sci. Eng., **124**(2), pp. 426–434.
[5] Neville, S. W., 1961, "Ultrasonic Welding," Br. Weld. J., **8**, pp. 177–187.
[6] Friswell, M. I., and Inman, D. J., 2000, "Sensor Validation for Smart Structures," J. Intell. Mater. Syst. Struct., **10**(12), pp. 973–982.
[7] Lee, S. S., Kim, T. H., Hu, S. J., Cai, W., Abell, J. A., and Li, J., 2012, "Characterization of Ultrasonic Metal Weld Quality for Lithium-Ion Battery Tab Joining," Proceedings of ASME Manufacturing Science and Engineering Conference, Notre Dame, IN, June 4–8.
[8] Lee, D., Kannatey-Asibu, E., Jr., and Cai, W., 2012, "Ultrasonic Welding Simulations for Multiple, Thin and Dissimilar Metals, Proceedings of ASME International Symposium on Flexible Automation, St. Louis, MO, June 18–20.
[9] Kim, T., Yum, J., Hu, S. J., Spicer, J. P., and Abell, J. A., 2011, "Process Robustness of Single Lap Ultrasonic Welding of Thin, Dissimilar Materials," CIRP Ann., **60**(1), pp. 17–20.
[10] De Vries, E., 2004, "Mechanics and Mechanisms of Ultrasonic Metal Welding," Ph.D. thesis, The Ohio State University, Columbus, OH.
[11] Du, H., and Klamecki, B. E., 1999, "Force Sensors Embedded in Surfaces for Manufacturing and Other Tribological Process Monitoring," ASME J. Manuf. Sci. Eng., **121**(4), pp. 739–748.
[12] Edelman, F., Gutmanas, E., and Brener, R., 1988, "Interfacial Processes and Diffusion in the Metal/Si_3N_4Si Thin-Film Systems," Isr. J. Technol., **24**(4), pp. 447–451.
[13] Foedinger, R., Rea, D., Sirkis, J., Wagreich, R., Troll, J., Grande, R., Davis, C., and Vandiver, T. L., 1998, "Structural Health Monitoring of Filament Wound Composite Pressure Vessels With Embedded Optical Fiber Sensors," Proceeding of the International SAMPE Symposium and Exhibition, Part 1 (of 2), Anaheim, CA, Vol. 43(1), pp. 444–457.
[14] Kodama, M., 1989, "Ultrasonic Welding of Non-Ferrous Metals," Weld. Int., **3**(10), pp. 853–860.
[15] Chang, U. I., and Frisch, J., 1974, "On Optimization of Some Parameters in Ultrasonic Metal Welding," Weld. J., **53**(1), pp. 24s–35s.
[16] Pfluger, A. R., and Sideris, X. N., 1975, "New Developments in Ultrasonic Welding," SAMPE Q., **7**(1), pp. 9–19.
[17] Hazlett, T. H., and Ambekar, S. M., 1970, "Additional Studies on Interface Temperatures and Bonding Mechanisms of Ultrasonic Welds," Weld. J., **49**(5), pp. 196s–200s.
[18] Cheng, X., and Li, X. C., 2007, "Investigation of Heat Generation in Ultrasonic Metal Welding Using Micro Sensor Arrays," J. Micromech. Microeng., **17**(2), pp. 273–282.
[19] Cheng, X., Datta, A., Choi, H., Zhang, X., and Li, X. C., 2007, "Study on Embedding and Integration of Micro Sensors Into Metal Structures for Manufacturing Applications," ASME J. Manuf. Sci. Eng., **129**(2), pp. 416–424.
[20] Zhang, X., Choi, H., Datta, A., and Li, X. C., 2006, "Design, Fabrication and Characterization of Metal Embedded Thin-Film Thermocouples With Various

Film Thicknesses and Junction Sizes," J. Micromech. Microeng., **16**(5), pp. 900–905.
[21] Choi, H., Datta, A., Cheng, X., and Li, X. C., 2006, "Microfabrication and Characterization of Metal-Embedded Thin-Film Thermomechanical Microsensors for Applications in Hostile Manufacturing Environments," J. Microelectromech. Syst., **15**(2), pp. 322–329.
[22] Cheng, X., Choi, H., Schwieso, P., Datta, A., and Li, X. C., 2005, "Micro Thin-Film Sensor Embedded in Metal Structures for In-Situ Process Monitoring During Ultrasonic Welding," North American Manufacturing Research Conference, NAMRC, Vol. 33, pp. 267–272.
[23] Choi, H., and Li, X. C., 2007, "Fabrication and Application of Micro Thin-Film Thermocouples for Transient Temperature Measurement in Nanosecond Pulsed Laser Micromachining of Nickel," Sens. Actuators, A, **136**(1), pp. 118–124.
[24] Datta, D., Choi, H., and Li, X. C., 2006, "Batch Fabrication and Characterization of Embedded Thin-Film Thermocouples in Metal," J. Electrochem. Soc., **153**(5), pp. H89–H93.